

## INFLUENCE OF STELLAR MULTIPLICITY ON PLANET FORMATION. II. PLANETS ARE LESS COMMON IN MULTIPLE-STAR SYSTEMS WITH SEPARATIONS SMALLER THAN 1500 AU

JI WANG<sup>1</sup>, DEBRA A. FISCHER<sup>1</sup>, JI-WEI XIE<sup>2</sup>, DAVID R. CIARDI<sup>3</sup>,(Received; Accepted)  
*to appear in ApJ*

## ABSTRACT

Almost half of the stellar systems in the solar neighborhood are made up of multiple stars. In multiple-star systems, planet formation is under the dynamical influence of stellar companions, and the planet occurrence rate is expected to be different from that for single stars. There have been numerous studies on the planet occurrence rate of single star systems. However, to fully understand planet formation, the planet occurrence rate in multiple-star systems needs to be addressed. In this work, we infer the planet occurrence rate in multiple-star systems by measuring the stellar multiplicity rate for planet host stars. For a sub-sample of 56 *Kepler* planet host stars, we use adaptive optics (AO) imaging and the radial velocity (RV) technique to search for stellar companions. The combination of these two techniques results in high search completeness for stellar companions. We detect 59 visual stellar companions to 25 planet host stars with AO data. Three stellar companions are within 2'', and 27 within 6''. We also detect 2 possible stellar companions (KOI 5 and KOI 69) showing long-term RV acceleration. After correcting for a bias against planet detection in multiple-star systems due to flux contamination, we find that planet formation is suppressed in multiple-star systems with separations smaller than 1500 AU. Specifically, we find that compared to single star systems, planets in multiple-star systems occur  $4.5 \pm 3.2$ ,  $2.6 \pm 1.0$ , and  $1.7 \pm 0.5$  times less frequently when a stellar companion is present at a distance of 10, 100, and 1000 AU, respectively. This conclusion applies only to circumstellar planets; the planet occurrence rate for circumbinary planets requires further investigation.

*Keywords:*

## 1. INTRODUCTION

The majority of the stars in the solar neighborhood belong to multiple-star systems (Duquennoy & Mayor 1991; Fischer & Marcy 1992; Raghavan et al. 2010; Duchêne & Kraus 2013). In multiple-star systems, many planets have been detected. Some planets are detected in circumbinary orbits (P-type, Dvorak 1982), where the planet orbits both stars (e.g., Doyle et al. 2011; Welsh et al. 2012; Schwamb et al. 2013). Some others are detected in circumstellar orbits (S-type), where the planet orbits only one of the stars (e.g., Cochran et al. 1997; Eggenberger et al. 2004). Compared to our statistical knowledge of planets around single stars (Cumming et al. 2008; Howard et al. 2010; Mayor et al. 2011; Wright et al. 2012; Mann et al. 2012; Dressing & Charbonneau 2013; Gaidos 2013; Swift et al. 2013; Kopparapu 2013; Petigura et al. 2013; Petigura et al. 2013; Bonfils et al. 2013; Parker & Quanz 2013), our understanding of planet formation in multiple-star systems is rather limited; the planet occurrence rate in multiple-star systems is still largely

unconstrained.

Planets in multiple-star systems can be studied by either searching for planets in known multiple-star systems, or searching for stellar companions in known planetary systems. There have been a few studies to search for planets in known multiple-star systems (e.g., Konacki 2005; Eggenberger & Udry 2007; Konacki et al. 2009; Toyota et al. 2009). However, this direct method is prone to flux contamination of stellar companions, which affects measurement precision (Wright et al. 2012). In comparison, the technical challenges are dramatically reduced for detecting stellar companions in known planetary systems; it is easier to search for a star than it is to search for a planet. Determination of the stellar multiplicity rate for planet host stars solves the inverse problem of measuring the planet occurrence rate in multiple-star systems (Wang et al. 2014). If planet host stars are rarely in multiple-star systems, this would indicate a low planet occurrence rate in these systems.

There have been numerous studies which have measured the stellar multiplicity rate of planet host stars. Most of these studies used imaging techniques, such as the adaptive optics (AO) imaging (Luhman & Jayawardhana 2002; Patience et al. 2002; Eggenberger & Udry 2007; Eggenberger et al. 2011; Adams et al. 2012, 2013; Law et al. 2013; Dressing et al. 2014), Lucky Imaging (Daemgen et al. 2009; Ginski et al. 2012; Lillo-Box et al. 2012; Bergfors et al. 2013;

Electronic address: ji.wang@yale.edu

<sup>1</sup> Department of Astronomy, Yale University, New Haven, CT 06511 USA<sup>2</sup> Department of Astronomy & Key Laboratory of Modern Astronomy and Astrophysics in Ministry of Education, Nanjing University, 210093, China<sup>3</sup> NASA Exoplanet Science Institute, Caltech, MS 100-22, 770 South Wilson Avenue, Pasadena, CA 91125, USA

Lillo-Box et al. 2014), speckle imaging (Horch et al. 2012; Kane et al. 2014), wide field imaging (Mugrauer et al. 2007; Mugrauer & Neuhauser 2009), HST imaging (Gilliland et al. 2014), and other techniques (Raghavan et al. 2006, 2010; Roell et al. 2012). These studies have mostly reached similar conclusions that the stellar multiplicity rate of planet host stars is lower than or comparable to that for field stars in the solar neighborhood. Among these studies, some focused on stars hosting planets detected in ground-based RV or transiting surveys (Luhman & Jayawardhana 2002; Patience et al. 2002; Eggenberger et al. 2004; Raghavan et al. 2006; Mugrauer et al. 2007; Eggenberger & Udry 2007; Daemgen et al. 2009; Mugrauer & Neuhauser 2009; Raghavan et al. 2010; Roell et al. 2012; Ginski et al. 2012; Bergfors et al. 2013; Knutson et al. 2013). However, the bias of ground-based planet surveys is difficult to assess due to an unknown threshold for excluding multiple-star systems.

In comparison, the *Kepler* mission (Borucki et al. 2011; Batalha et al. 2013; Burke et al. 2014) did not strongly bias against multiple-star systems: (1), the low-angular-resolution *Kepler* Input Catalog images (Brown et al. 2011) did not reveal close binaries; (2), multiple-star systems (e.g., eclipsing binaries) received continued observation after detection. Therefore, the bias of ground-based surveys is not a major concern for studies of *Kepler* planet host stars (Lillo-Box et al. 2012; Adams et al. 2012; Horch et al. 2012; Adams et al. 2013; Law et al. 2013; Dressing et al. 2014; Kane et al. 2014; Gilliland et al. 2014; Lillo-Box et al. 2014). However, there is a detection bias against transiting planets in multiple-star systems. The transit depth is shallower due to the additional flux from stellar companions, which makes planet detection more difficult. This bias has to be taken into consideration when measuring the stellar multiplicity rate for planet host stars.

It is commonly accepted that planet formation may be disrupted in multiple-star systems with small separations (e.g.,  $\sim 10$ –200 AU). This is supported by both simulations (Th  bault et al. 2006; Jang-Condell 2007; Quintana et al. 2007; Paardekooper et al. 2008; Kley & Nelson 2008; Xie et al. 2010; Thebault 2011) and observations (Desidera & Barbieri 2007; Bonavita & Desidera 2007; Kraus et al. 2012). Therefore, surveys for gravitationally-bound stellar companions around planet host stars provides the best path for understanding planet formation in multiple-star systems. High-resolution imaging techniques are efficient for separations greater than  $0''.1$ , and spectroscopic measurements are efficient at detecting stellar companions at smaller separations.

To carry out this work, we select a sample of 56 stars hosting planet candidates from the *Kepler* mission to search for potential stellar companions using the RV and the AO imaging techniques. The RV technique is sensitive to short-period stellar companions, and the AO technique is sensitive to

those further out. The combination of these two techniques is sensitive to a larger range of semi-major axes, and results in a survey with much higher completeness than previous studies. We consider the detection bias against transiting planets in multiple-star systems, and correct for this when calculating the stellar multiplicity rate for planet host stars. We emphasize that we only consider planets in S-type circumstellar orbits.

The paper is organized as follows. We describe our sample and the sources for their RV and AO data in §2. In §3, we present the analyses of available data: searching for stellar companions to planet host stars using the RV and AO techniques. In §4, we introduce a method of correcting for detection bias against planets in multiple-star systems, and apply it to the measurement of stellar multiplicity rate for planet host stars. We then calculate the planet occurrence rate for single and multiple star systems by comparing their multiplicity rates. Discussion and summary are given in §5.

## 2. SAMPLE DESCRIPTION AND DATA SOURCES

RV and AO data are provided by the *Kepler* Community Follow-up Observation Program<sup>4</sup> (CFOP). Since RV data are critical for probing stellar companions on close orbits, we select 56 *Kepler* Objects of Interest (KOIs) with at least 3 RV data points, for which the long-term RV acceleration due to a stellar companion may be measured. The RV data were taken with the HIRES instrument (Vogt et al. 1994) at the Keck I telescope, and reported in Marcy et al. (2014).

The AO data for these 56 KOIs were taken at different observatories including Keck, MMT, Gemini, Lick, Palomar, and WIYN. A summary of the sample and data sources is given in Table 1. Information on KOIs is provided by the NASA Exoplanet Archive (NEA, Huber et al. 2014)<sup>5</sup>. All the stars in our sample are solar-type stars with effective temperature ( $T_{\text{eff}}$ ) in the range between 4725 K and 6300 K, and surface gravity ( $\log g$ ) in the range of 3.9 and 4.7. There are 27 (48% of the sample) multi-planet systems.

## 3. DETECTIONS AND CONSTRAINTS ON STELLAR COMPANIONS TO PLANET HOST STARS

We use three techniques to detect and constrain stellar companions around planet host stars: the RV technique (§3.1), the AO imaging technique (§3.2), and the dynamical analysis (DA, §3.3). These three techniques are complementary and sensitive to different parts of parameter space. The RV technique is sensitive to close-in companions with small to intermediate mutual inclinations with respect to the planet orbital planes; the DA technique is sensitive to companions at large mutual inclinations; and the AO imaging technique is sensitive to stellar companions at larger separations. We will discuss in this section how we use these techniques to detect stellar companions and constrain their presence.

<sup>4</sup> <https://cfop.ipac.caltech.edu>

<sup>5</sup> <http://exoplanetarchive.ipac.caltech.edu/>

### 3.1. RV Detections and Completeness

We use the Keplerian Fitting Made Easy (KFME) package (Giguere et al. 2012) to analyze the RV data. The procedure are described as follows. We first calculate the root mean square ( $\text{RMS}_1$  in Table 2) of the the RV data. If  $\text{RMS}_1$  is five times higher than the median reported RV uncertainties,  $\delta v$ , then we mark a variability flag. For systems marked with variability flags, we first fit the RV data with a linear trend, or a long-period orbit due to a non-transiting object. The systems with a significant linear trend ( $3\sigma$ ) or the signal of an additional non-transiting object will be marked with a slope flag or a non-transiting component flag. The linear trend or the long-period orbit is then removed.

For the RV residuals after removing the linear trend or the long-period orbit, and the RVs for systems with no variability flag, we consider two cases. First, if the system has only one detected KOI, then we fit the RV data with a circular Keplerian orbit allowing only the RV semi-amplitude to change. If the resulting RMS ( $\text{RMS}_2$ ) is smaller than  $\text{RMS}_1$ , then  $\text{RMS}_2$  is used in subsequent analyses; otherwise  $\text{RMS}_1$  is used. Second, if the system has multiple KOIs, then we choose the one KOI causing the largest RV variation. When deciding which planet in the KOI causes the largest RV variation, we assume the planet mass-radius relationship from Lissauer et al. (2011), and calculate the nominal RV amplitude for each planet. Then we fit the RV data with a circular Keplerian orbit allowing only the RV semi-amplitude to change. The minimum of  $\text{RMS}_1$  and  $\text{RMS}_2$  is used in subsequent analyses. In the above process, fitting eccentric orbit does not significantly change the RMS. In addition, including more KOIs for multi-planet systems does not always help to reduce the RMS because of large RV measurement uncertainty relative to the small RV signals of small planets.

Among 56 stars, only one shows a long-term RV slope: KOI 69 has a RV linear trend of  $12.2 \pm 0.2 \text{ ms}^{-1} \text{ yr}^{-1}$ . During 4.1 years of RV measurements, there is no sign of deviation from the linear trend, indicating that the companion is at least 4 AU away. More discussion regarding this system will be given in §3.2 after considering the AO data. Six systems have non-transiting objects revealed by the RV data: KOI 5, KOI 104, KOI 148, KOI 244, KOI 246, and KOI 1442. The latter five are known non-transiting planets (Marcy et al. 2014). KOI 5 shows a parabolic acceleration, but the period of the non-transiting object is unconstrained. We will discuss KOI 5 more in §3.2 with the addition of AO data. For 15 cases, RMS is still 5 times higher than the reported RV measurement uncertainty after considering a non-transiting object, or the KOI planet dominating the RV variability. The “excessive” RV variability may be attributed to the following factors or their combinations: very limited number of RV data points, an underestimated RV measurement uncertainty, excessive stellar activity, and additional stellar or planetary components. We find that 12 out of the 15 KOIs with “excessive” RV vari-

ation have fewer than 21 RV measurements, which is the median number of RV measurements for the 56 KOIs in our sample. Seven of them have fewer than 10 RV measurements. The limited number of RV measurements would result in an improper RV orbital fitting, which leads to a higher RMS. In addition, RV jitter is not considered in the reported RV uncertainty in Table 2. After considering a typical RV jitter of  $1\text{--}3 \text{ m}\cdot\text{s}^{-1}$  for Kepler stars with RV measurements (Marcy et al. 2014), 10 out of the 15 KOIs with “excessive” RV variation have less than 5 times of the RV uncertainty. KOI 22 remains the only KOI in our sample with “excessive” RV variation that cannot be explained by either the limited number of RV measurements or stellar activity.

We study the completeness of searching for stellar companions by simulations following the subsequent procedures. We first define a parameter space,  $a - i$  space, where  $a$  is the separation of a companion star, and  $i$  is the mutual inclination of the sky plane and the companion star orbital plane. We divide the parameter space into many fine grids ( $\Delta a = 0.5 \text{ AU}$ ,  $\Delta i = 10^\circ$ ). For each star, we simulate 1000 companion stars on each grid, and count how many simulated companion stars are detected given the time baseline, observation epochs, and measurement uncertainties of the RV data. Specifically, we generate a synthetic RV data set for each of the simulated companion stars. Observation epochs and measurement uncertainties remain the same as the original RV data. If the RMS of the synthetic RV data is 3 times larger than the observed RV RMS, i.e., the smaller of  $\text{RMS}_1$  and  $\text{RMS}_2$ , then we count the simulated stellar companion as a detection. The separation and mass ratio distributions of simulated stellar companions follow the normal distributions reported in Duquennoy & Mayor (1991), i.e.,  $\log_{10} a = 1.49$ ,  $\sigma_{\log_{10} a} = 1.54$ ;  $q = m_2/m_1 = 0.23$ ,  $\sigma_q = 0.42$ . We use the median orbital eccentricity for binary stars ( $e = 0.4$ , Duquennoy & Mayor 1991) and a random periastron distribution in simulations. The median completeness contours are shown in Fig. 1. RV completeness drops to below 50% as separations become larger than 30 AU.

In summary, RV observations of 56 stars reveal 7 non-transiting companions, 5 of these are previously-reported planets (Marcy et al. 2014). Orbits of the other two are unconstrained because of limited RV baselines. KOI 5 shows a parabolic RV acceleration, and KOI 69 shows a linear RV trend of  $12.2 \pm 0.2 \text{ ms}^{-1} \text{ yr}^{-1}$ . The nature of these two companions will be discussed more in the following section.

### 3.2. AO Detections and Completeness

The RV variation of most of stellar companions at larger separations is difficult to measure because of the long periodicity. However, the AO imaging technique is more effective in constraining stellar companions at larger separations. We will discuss in the following part how we detect and characterize stellar companions based on AO images.



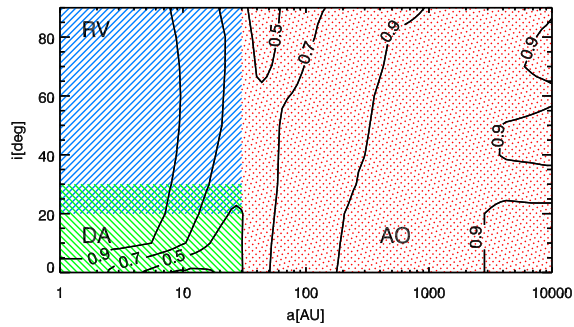


**Figure 1.** Median completeness contours for 3 techniques used to detect and constrain stellar companions to planet host stars. These 3 techniques are sensitive to different part of the  $a-i$  parameter space. The radial velocity (RV) technique is sensitive to stellar companions within  $\sim 30$  AU and with small or intermediate mutual inclinations to planet orbital planes (blue hatched region). The dynamical analysis (DA) technique is sensitive to a similar range of separations but larger mutual inclinations (green hatched region). The adaptive optic (AO) technique is sensitive to stellar companions at wider orbits (red dotted region). The combination of these 3 techniques contributes to a survey of stellar companions with high completeness.

### 3.2.1. Contrast Curve

The contrast curve of an image provides detection thresholds for detecting faint companions around a star. The procedures of calculating the contrast curve are described as follows. We define a series of concentric annuli, centered on the star, for which we calculate the median and the standard deviation of flux for pixels within these annuli. We use the value of 5 times the standard deviation above the median as the  $5\text{-}\sigma$  detection limit. The contrast curve is the  $5\text{-}\sigma$  detection limit as a function of the radii of concentric annuli. The median contrast curve and the  $1\text{-}\sigma$  deviation of the AO images we use in this paper are shown in Fig. 2, where each pixel is converted into angular separation based on plate scale of each instrument:  $0''.010/\text{pixel}$  for Keck NIRC2 (Wizinowich et al. 2000),  $0''.011/\text{pixel}$  for Gemini DSSI<sup>6</sup>,  $0''.019/\text{pixel}$  or  $0''.038/\text{pixel}$  for MMT ARIES (Sarlot et al. 1999),  $0''.025/\text{pixel}$  for Palomar PHARO (Hayward et al. 2001),  $0''.075/\text{pixel}$  for Lick IRCAL (Lloyd et al. 2000),  $0''.017\text{--}0''.018/\text{pixel}$  for WIYN DSSI (Horch et al. 2009), and  $0''.043/\text{pixel}$  for Palomar Robo-AO (Law et al. 2013).

### 3.2.2. Distance Estimation

In order to obtain the physical projected separation between detected companions and the central stars, we need to estimate the distance. The distance of a star can be measured with the distance modulus and an estimation of extinction. The extinction estimation in the  $V$  band ( $A_V$ ) is obtained from the Mikulski Archive for Space Telescopes (MAST)<sup>7</sup>. Details of  $A_V$  estimation can be found in §6 and §7 in Brown et al. (2011). The distance modulus is the magnitude difference between

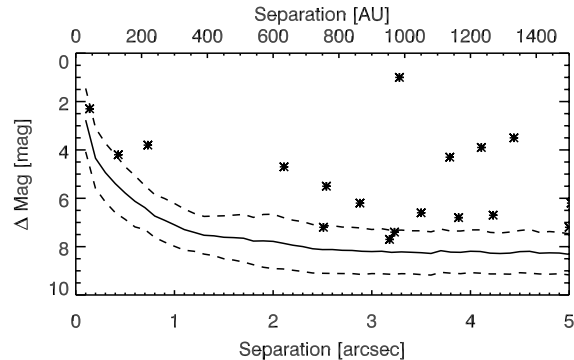


**Figure 2.** Median contrast curve for the AO images. Dashed lines are  $1\text{-}\sigma$  deviation of the contrast curve. Detections within  $5''$  are shown as asterisks. Physical projected separation in AU is calculated assuming the average distance of the sample, i.e., 300 pc. When analyzing the detection completeness, each star in our sample is treated individually for the observation band in which the AO image was taken. A total of 59 visual companions around 25 planet host stars are detected (Table 3).

the apparent magnitude and the absolute magnitude in the  $V$  band. The apparent  $V$  magnitude is calculated based a conversion from  $g'$  and  $r'$  magnitudes (Smith et al. 2002). The absolute  $V$  magnitude is estimated with the Yale-Yonsei (Y2) stellar evolution model (Demarque et al. 2004): with  $T_{\text{eff}}$ ,  $\log g$ , age, and  $[\text{Fe}/\text{H}]$  measured from spectroscopic and/or asteroseismic observations, the absolute  $V$  magnitude can be estimated from the Y2 interpolator. For stars with an unknown  $A_V$ , which is the case for 7 stars, we use the distance modulus in  $K$  band to estimate the distance with the assumption that  $K$  band extinction is much smaller than  $V$  band for *Kepler* stars. Distances for KOIs with visual stellar companion detections are provided in Table 3.

### 3.2.3. Detection and Completeness

Based on the images from the CFOP, we detect a total of 59 visual stellar companions around 25 planet host stars (Table 3). Fourteen stars (25%) have stellar companions within a  $5''$  radius. The closest companion has a projected separation of 40.9 AU ( $0''.14$ ) from KOI 5.

The 56 stars in our sample have an average distance of  $\sim 300$  pc. Given the contrast curve shown in Fig. 2, the search for stellar companions closer than  $\sim 40$  AU and low-mass stars ( $\Delta \text{Mag} > 8$ ) is not complete. We therefore conduct simulations to evaluate the completeness of the AO survey. Similar to the RV completeness simulations in §3.1, we artificially generate 1000 companion stars at each predefined grid in the  $a-i$  parameter space. If the contrast ratio ( $\Delta \text{Mag}$ ) between a simulation star and the central star is smaller than the value given by AO  $5\text{-}\sigma$  contrast curve, then we record it as a detection. Note that the contrast curves used in simulations are those calculated for each individual star in the observed band rather than the median contrast curve shown in Fig. 2. The AO completeness contours (median of 56 stars) are plotted in Fig. 1. From this plot, we show that the AO completeness

<sup>6</sup> <http://www.gemini.edu/sciops/instruments/dssi-speckle-camera-north>

<sup>7</sup> <https://archive.stsci.edu/>

is less than 50% for separations smaller than  $\sim 40$  AU. At smaller separations, the RV technique becomes a much more efficient way of detecting stellar companions.

### 3.2.4. KOI 5

KOI 5 has a parabolic RV acceleration indicating a distant companion, but the orbit of this companion is unconstrained given only  $\sim 4$  years' observation and the poor phase coverage. There are many possible orbital solutions given the current RV data. Fig. 3 shows two examples. If the RV acceleration is caused by the stellar companion detected by the AO imaging, then it requires a highly eccentric orbit ( $e = 0.92$ ) to reasonably fit the RV data. We estimate the mass of the AO detected stellar companion to be  $\sim 0.5 M_{\odot}$  based on its differential magnitude in the  $K$  band (Kraus & Hillenbrand 2007). Alternatively, the observed RV acceleration can be explained by a stellar companion ( $0.08 M_{\odot}$ ) at 7 AU separation on a circular orbit. Any solutions with separations smaller than 7 AU should involve companions that fall into sub-stellar mass regime. Therefore, we conclude that a stellar companion may exist around KOI 5, but with a separation larger than 7 AU (i.e.,  $0''.024$  angular separation).

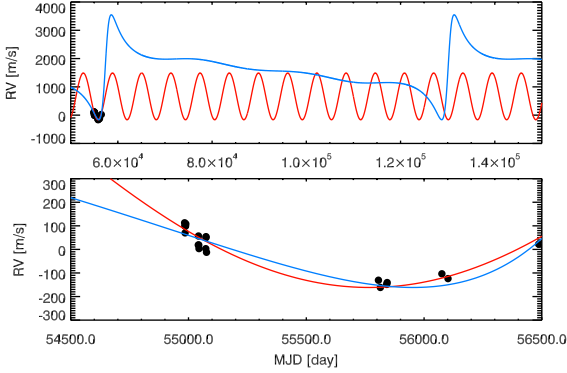


**Figure 3.** Two possible scenarios for the observed RV acceleration of KOI 5. Black dots are current RV data. Blue line shows a case in which the RV acceleration is caused by the AO detected companion with a 40.9 AU projected separation (i.e.,  $0''.14$  angular separation). A highly eccentric orbit ( $e = 0.92$ ) is required to reasonably fit the RV data. Red line shows another case in which a  $0.08 M_{\odot}$  companion on a circular orbit with a 7 AU separation causes the RV acceleration. More RV data with a longer baseline are required to determine the nature of the companion causing the RV acceleration of KOI 5. Top panel shows a large time range, and the bottom panel shows a zoom-in plot to a time range with RV data.

### 3.2.5. KOI 69

KOI 69 shows a linear RV trend of  $12.2 \pm 0.2 \text{ m s}^{-1} \text{ yr}^{-1}$ , which can be caused either by a more distant star or a closer sub-stellar object. Fig. 4 shows possible parameter space for this companion. RV data exclude any companions below the straight solid line because they are not massive enough to cause the trend. Although AO data shows non-detection for KOI 69, the AO contrast curve can

put constraint on any bright stellar objects which would have been detected. After considering the constraints from AO and RV observations, if the companion causing the RV linear trend is a star, it is mostly likely to lie between 15.5 and 33.0 AU (i.e.,  $0''.18$  and  $0''.38$  in angular separation), and its mass cannot exceed 102 Jupiter mass ( $2\sigma$ ). If the companion mass is in the sub-stellar regime, its mass and separation is confined to a parallelogram marked as “Sub-stellar” in Fig. 4. The 4 vertices of the parallelogram are (5.5 AU,  $10.0 M_J$ ), (9.8 AU,  $10.0 M_J$ ), (27.6 AU,  $80.0 M_J$ ), and (15.5 AU,  $80.0 M_J$ ).

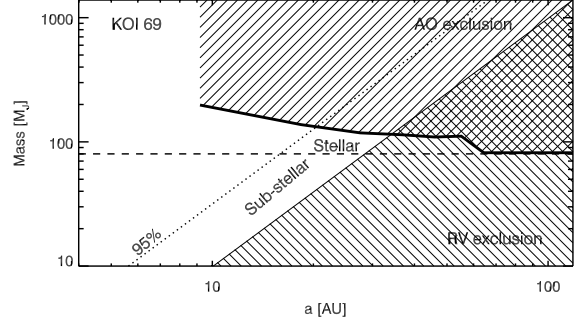


**Figure 4.** Parameter space for the companion to KOI 69 revealed by a RV linear trend. The region below the solid straight line is excluded because companions falling into this parameter space are not massive and close enough to produce the observed RV linear trend. The solid thick line represents the contrast curve. Any stellar companions above the line would have been detected, so the parameter space above the solid thick line is also excluded. The dashed line divides the stellar regime and sub-stellar regime. The dotted line represents the 95 percentile of the solutions given the linear RV trend, i.e., 95% of the solutions should fall in between the solid straight line and the dotted line assuming a random orbital orientation of the companion. If the linear RV trend is caused by a stellar companion, then it is most likely the case that the separation is between 15.5 and 33.0 AU, as confined in a parameter space noted with “Stellar”.

### 3.2.6. Visual Companions Association

We detect 59 visual companions around 25 planet host stars, but we do not know whether they are associated or bonded to the host stars. Lillo-Box et al. (2012) estimated  $\sim 35\%$ - $53\%$  of visual companions are bonded to the primary stars within  $3''$ , and this ratio decreases with increasing angular separations. Therefore, a non-negligible fraction of visual companions we detect are in fact unassociated to primary stars, which will decrease the stellar multiplicity rate for planet host stars.

For 12 visual companions with multi-band detections (i.e.,  $J$  and  $K$  band), we test if they are physically associated with their primary stars. The procedures of the test are described as follows. We calculate the  $J$ - $K$  colors of visual companions based on the differential magnitudes in Table 3 and the  $J$ - $K$  colors of primary stars from the NEA. From their  $J$ - $K$  colors, we interpolate for the absolute  $K$  band magnitude of companion stars based on Table 5 in Kraus & Hillenbrand (2007). With the absolute  $K$  band magnitudes and the apparent  $K$  band

magnitudes, we calculate the distances of the visual companion stars, and check whether they are consistent with the distances of the primary stars. If the color-determined distance for the companion is  $1\sigma$  different from the distance of the KOI as reported in Table 3, we reject the physical association between the KOI and the visual companion star. We find inconsistent distance for 6 out of 12 visual companions. The 6 companions include one for KOI 87 (at  $5''.49$  separation,  $d = 2.9 \pm 2.2$  kpc), one for KOI 153 (at  $6''.17$  separation,  $d = 52 \pm 44$  kpc), one for KOI 244 (at  $8''.40$  separation,  $d = 33 \pm 20$  pc), and all three for KOI 377 ( $d = 3.8 \pm 2.2$  kpc,  $d = 204 \pm 163$  kpc, and  $d = 412 \pm 330$  kpc).

### 3.3. Dynamical Analysis

In addition to constraints from RV and AO data, more constraints of potential stellar companions can be put on multi-planet systems (Wang et al. 2014). There are 27 (48% of the sample) multi-planet systems in our sample for which we can apply the dynamical analysis (DA). The DA technique makes use of the co-planarity of multi-planet systems discovered by the *Kepler* mission (Lissauer et al. 2011). A stellar companion with high mutual inclination to the planetary orbits would have perturbed the orbits and significantly reduce the co-planarity of planetary orbits, and hence the probability of multi-planet transits. Therefore, the fact that we see multiple planet transiting helps to exclude the possibility of a highly-inclined stellar companion. The DA is complementary to the RV technique because it is sensitive to stellar companions with large mutual inclinations to the planetary orbits. The parameter space the DA is sensitive to is shown in Fig. 1.

### 3.4. Combining Results From Different Techniques

For the RV and AO observations, detection completeness contours are calculated based on simulations given the observational constraints, such as the time baseline, cadence, measurement uncertainties, and the contrast curve. For the DA technique, numerical integrations give the fraction of time when multiple planets can stay with small mutual inclinations ( $< 5^\circ$ ) so that multiple transiting planets can be observed (Wang et al. 2014). Note that the DA technique works only for systems with multiple planets, which account for 48% of the sample. For systems with a single transiting planet, no constraint can be given by the DA technique. We denote  $c_{RV}$ ,  $c_{AO}$  and  $c_{DA}$  as the completenesses at a given point in the  $a-i$  parameter space, overall completeness  $c$  is equal to  $1 - (1 - c_{RV}) \times (1 - c_{AO}) \times (1 - c_{DA})$ . We note that the calculation assumes each technique is independent and uniquely sensitive to a certain portion of the parameter space. This is generally the case since the RV technique completeness drops quickly beyond  $\sim 30$  AU, where the AO technique sensitivity is high. Similarly, the RV and DA techniques and the DA and AO techniques have little overlap in sensitivity parameter space. The overall completeness may be overestimated at the transition space,

such as  $a = 30$  AU (for RV and AO) and  $i = 20^\circ$  (for RV and DA), because stellar companions falling into this parameter space can be detected by multiple techniques and thus the techniques become correlated. We also try another way of combining results from different techniques, in which we use the maximum completeness as the overall completeness. This approach assumes multiple techniques are correlated, however, it does not significantly change the conclusions in this paper.

The completeness is then integrated over the  $a-i$  parameter space. We assume a log-normal distribution for  $a$  (Duquennoy & Mayor 1991; Raghavan et al. 2010), random distribution of  $i$  for systems with only one transiting planet, and the  $i$  distribution from Hale (1994) for systems with multiple transiting planets. The treatment for multiple transiting planet systems is detailed in Wang et al. (2014), i.e., a coplanar distribution for stellar companions within 15 AU, a random  $i$  distribution for stellar companions beyond 30 AU, and a mixture  $i$  distribution at intermediate separations between 15 and 30 AU.

## 4. PLANET OCCURRENCE RATE AND STELLAR MULTIPLICITY RATE

### 4.1. Detection Bias Against Planets in Multiple-Star Systems

Planets in multiple-star systems are more difficult to find using the transiting method because of flux contamination. We discuss how this bias against planet detection in multiple-star systems can be quantified. For the *Kepler* mission, it is a necessary condition to become a planet candidate that the signal to noise ratio (S/N) should be higher than 7.1 (Jenkins et al. 2010a). S/N can be calculated using the following equation:

$$S/N = \frac{\delta}{CDPP_{\text{eff}}} \sqrt{N_{\text{transits}}}, \quad (1)$$

where  $\delta$  is the transit depth,  $CDPP_{\text{eff}}$  is the effective combined differential photometric precision (Jenkins et al. 2010b), a measure of photometric noise, and  $N_{\text{transits}}$  is the number of observed transits. We use a planet in a binary system as an example to calculate the transit depth:

$$\delta = \frac{R_{\text{PL}}^2}{R_*^2} \frac{F_*}{F_* + F_c}, \quad (2)$$

where  $R_{\text{PL}}$  is planet radius,  $R_*$  is the radius of the star that the planet is transiting,  $F$  denotes flux, and subscript  $*$  and  $c$  indicate the planet host star and the contaminating star, respectively. Two cases are considered for the above equation. First, if the planet transits the primary star, the transit depth is diluted by a factor of 2 at most, when  $F_*$  and  $F_c$  are identical. Second, if the planet transits the secondary star, the transit depth dilution effect due to flux contamination can be much larger than 2 even after considering the increase in the transit depth from a reducing  $R_*$  in the first term of the equation. For an example of a solar-type star and a late-type M dwarf pair, the gain of a reducing  $R_*$  can be a

factor of 100 at most, but the flux ratio between the two stars can easily exceed  $10^4$  in the *Kepler* band.

Therefore, we conduct simulations to quantify the detection bias against planets in binary star systems. For each KOI, we choose the one planet that gives the highest S/N. We add a companion star in the system and calculate the S/N in the presence of flux contamination for two cases: planet transiting the primary star and planet transiting the secondary star. In both cases, we assume the same period and transit duration from the NEA so that  $CDPP_{\text{eff}}$  and  $N_{\text{transits}}$  in Equation 1 are the same, and flux contamination (see Equation 2) is the only factor that determines whether a planet is detected in the presence of a companion star. If the S/N is higher than 7.1, then the planet can still be detected by *Kepler*, but with a lower significance. We randomly assign a stellar companion (secondary star) to a KOI (primary star) and repeat this procedure 1000 times for both the primary and the secondary star. We record the fraction of planet detections,  $\alpha$ , which will be used in correcting for the bias of detecting planets in multiple-star systems (Table 4). The median value of  $\alpha$  for 56 stars in our sample is 0.89, implying that the detection bias is not severe, but certainly not negligible.

In the simulations, we use the stellar parameters from the NEA for the primary star. When generating a stellar companion in the simulations, we assume the mass ratio distribution follows the normal distribution given in Duquennoy & Mayor (1991). The radius of the secondary star is calculated using a stellar mass-radius relationship (Feiden & Chaboyer 2012). Estimation of stellar flux for both primary and secondary stars are based on Table 5 in Kraus & Hillenbrand (2007). We calculated  $CDPP_{\text{eff}}$  by interpolating between 3, 6, and 12-hour  $CDPP$ s based on transit duration.

#### 4.2. Distinguishing Planets in Single and Multiple-Star Systems

The *Kepler* mission has provided us with a large sample of planet candidates. However, we do not know whether the planet host stars are in single or multiple stellar systems. Distinguishing planets in single and multiple-star systems allows us to separately calculate the planet occurrence rate for these two types of stars, and to understand planet formation in different stellar environments (Wang et al. 2014). Follow-up observations are critical in identifying additional stellar companions in planetary systems. Even in the case of non-detection, with RV, AO, and DA techniques, we can calculate the probability of a star being in a multiple-star system based on the completeness study. For example, if the overall completeness for a companion detection is 80% and the stellar multiplicity rate is 46% (Raghavan et al. 2010), then the probability of the star having an undetected companion (or being a multiple-star) is  $(100\%-80\%) \times 46\% = 0.092$ . Following this procedure, we calculate the number of multiple-stars  $N_M$  and the number of single stars  $N_S$ . Since  $N_M$  and  $N_S$  are the sums of probabili-

ties, they will not necessarily be integers:

$$N_M = \sum_{i=1}^n [p_M(i)/\alpha(i)], \quad N_S = \sum_{i=1}^n [1 - p_M(i)], \quad (3)$$

where  $n$  is the total number of stars in the sample,  $p_M(i)$  is the probability of the  $i_{\text{th}}$  star being a multiple-star system,  $\alpha(i)$  is the correction factor for the detection bias for planets in multiple-star systems. The above equation is similar to Equation 6 in Wang et al. (2014) except for the correction factor  $\alpha$ . Note that there is an implicit correction factor for single stars in Equation 3. However, the correction factor for single stars is 1. If a stellar companion is detected for a KOI, then  $p_M$  is assigned to 1, and  $\alpha$  is also assigned to 1 because no bias exists in this case since a planet has already been detected in a multiple-star system. For an AO detected stellar companion, setting  $p_M$  to 1 is an overestimation because the physical association of visual stellar components is not yet established. Therefore, the stellar multiplicity rate that will be subsequently determined is an upper limit.

We then define  $f$  as the fraction of stars with planets,  $f$  can be separated into two components:

$$f = (1 - \text{MR}) \times f_S + \text{MR} \times f_M, \quad (4)$$

where MR is the global stellar multiplicity rate,  $f_S$  and  $f_M$  are the fraction of stars with planets for single and multiple-star systems, respectively. The ratio of  $f_S$  and  $f_M$  can be calculated in the following equation:

$$\frac{f_S}{f_M} = \frac{\frac{N_S}{1 - \text{MR}}}{\frac{N_M}{\text{MR}}}. \quad (5)$$

With Equation 4 and 5,  $f_S$  and  $f_M$  can be solved independently given that  $N_S$  and  $N_M$  can be measured and that  $f$  can be measured globally (e.g., Fressin et al. 2013). In addition, the MR for planet host stars ( $\text{MR}_{\text{PL}}$ ) can be calculated and compared to a global MR:

$$\text{MR}_{\text{PL}} = \frac{N_M}{N_M + N_S}, \quad (6)$$

#### 4.3. Stellar Multiplicity Rate For Planet Host Stars

Fig. 5 shows the comparison between the stellar multiplicity rate for field stars (dashed line Duquennoy & Mayor 1991; Raghavan et al. 2010) and that for planet host stars (blue and red hatched regions). The red hatched region is the  $1-\sigma$  uncertainty region for 56 stars with RV and AO observations, and the DA analysis. The error bar of  $N_M$  is estimated based on Poisson statistics. The square root of the closest integer to  $N_M$  is used as the error bar to  $N_M$  unless the closest integer is zero, in which case we used 1 for the error of  $N_M$ . The stellar multiplicity rate for planet host stars is significantly lower than that of field stars until the separation reaches  $\sim 1500$  AU. This implies that the influence of a stellar companion may be more profound than



previously thought. The effective separation below which planet formation is significantly affected is extended to  $\sim 1500$  AU. In comparison, the blue hatched region represents the  $1-\sigma$  uncertainty region for 23 stars with RV data and DA analysis, but no AO observations (Wang et al. 2014). Based on the blue hatched region, the significant difference of stellar multiplicity disappears after separation reaches 20.8 AU. Since Wang et al. (2014), we have incorporated AO data into our analyses and increased the sample size from 23 to 56. These improvements greatly strengthen the statistics in the comparison. Specifically, increasing the sample size reduces the statistical uncertainty; adding AO data helps constrain stellar companions beyond the reach of the RV technique.

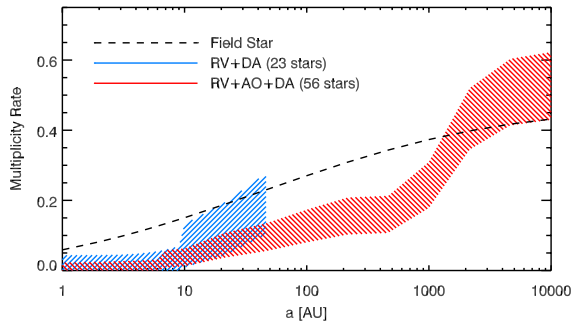


**Figure 5.** Comparison of stellar multiplicity rate between field stars (dashed line) and planet host stars (hatched regions). Blue hatched region represents the  $1-\sigma$  region of the stellar multiplicity rate for 23 planet host stars with RV and DA analysis (Wang et al. 2014). AO data were not incorporated, so the sensitivity of RV and DA was limited within 50 AU. For this study, AO data are used to constrain stellar companions beyond 50 AU. Red hatched region represents the  $1-\sigma$  region of the stellar multiplicity rate for 56 stars with RV, AO and DA analysis. The new study shows that the stellar multiplicity rate for planet host stars is lower than that for the field stars within 1500 AU, indicating a more profound influence of stellar companions on planet formation.

#### 4.4. Planet Occurrence Rate vs. Binary Separation

With the stellar multiplicity rate for planet host stars, we can calculate the ratio of the planet occurrence rate for single and multiple-star systems according to Equation 5. Fig. 6 shows the ratio  $f_S/f_M$  as a function separation. Planets orbiting single stars are  $4.5 \pm 3.2$ ,  $2.6 \pm 1.0$ , and  $1.7 \pm 0.5$  times more likely than planets in S-type orbits in multiple-star systems with stellar separations of 10 AU, 100 AU, and 1000 AU, respectively. The deficiency of planets around multiple-stars indicates that the suppressive influence on planet formation of a stellar companion is significant at these separations. The suppressive effect decreases as separation increases, and  $f_S$  and  $f_M$  are comparable at separations around  $\sim 1500$  AU, indicating that stellar companions at these separations barely have any influence on planet formation. The comparison of planet occurrence rate for single and multiple-stars at other stellar separations is given in Table 5.

#### 4.5. Comparison to Previous Results

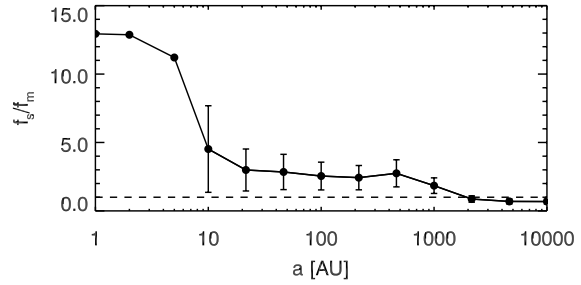


**Figure 6.** The ratio of the planet occurrence rates for single and multiple-stars. Dashed line represents the value of 1, a value indicating a comparable planet occurrence rate. The planet occurrence rate for single stars is much higher than that for multiple-stars within 10 AU. Beyond 10 AU, the ratios are  $4.5 \pm 3.2$ ,  $2.6 \pm 1.0$ , and  $1.7 \pm 0.5$  for 10 AU, 100 AU, and 1000 AU, respectively, indicating planets in multiple-star systems are fewer than those around single stars at these separations. The planet occurrence rates become comparable between single and multiple-stars when separation is larger than  $\sim 1500$  AU. Error bars are calculated based on Poisson statistics and propagated through Equation 5. No error bar is shown within 10 AU because of less than 1 detection of stellar companion according to Equation 3.

The field of studying planets in multiple-star systems may be divided into two eras: before and after the *Kepler* mission. Before the *Kepler* mission, stars with giant planets are the main targets, and they are mostly detected by the RV technique. Bonavita & Desidera (2007) used a sample defined as the “uniform detectability” (UD) sample. They searched for stellar companions around stars in this sample, and found that the fractions of stars with detected planets are comparable between single and multiple-stars. However, after considering the search incompleteness, they concluded that the frequency of planets in binary stars cannot be more than a factor of 3 lower than that for single stars. Their finding is consistent with our conclusion for separations larger than  $\sim 50$  AU. However, we find that  $f_S/f_M$  can be higher than 3 for shorter binary separations (Table 5). Eggenberger et al. (2011) presented comparison of stellar multiplicity rate between planet host stars and a control sample of non-planet host stars. They concluded that S-type gas giant planets are less frequent in binary stars with mean semi-major axes between 35 and 250 AU. Their conclusion is qualitatively consistent with ours, but we find that planet formation can be suppressed at larger separations (out to 1500 AU). We emphasize that there are fundamental differences in the comparison to previous results on RV planet surveys. First, they focused on host stars of gas giant planets, whereas this study has made use of *Kepler* data, and therefore mostly deals with lower-mass planets. Second, RV surveys have a much stronger bias against close-in binary stars than the *Kepler* mission.

After the *Kepler* satellite was launched, studies continue on the stellar multiplicity of planet host stars. Lillo-Box et al. (2012) found that the visual companion rate for KOIs is 17.3% and 41.8% within  $3''$  and  $6''$ , respectively. They later updated the companion rate to be 17.2% and 32.8% within  $3''$  and  $6''$  (Lillo-Box et al. 2014). Dressing et al.



(2014) found that 17.2% of KOIs have visual companions within  $3''$ . In comparison, we find that  $12.5 \pm 4.7\%$  and  $48.2 \pm 9.3\%$  of KOIs have visual companions within  $3''$  and  $6''$ , which is consistent with their numbers. Adams et al. (2012) found that 60%, 20%, and 7% of 90 KOIs have stellar companions within  $6''$ ,  $2''$ , and  $0''.5$ , respectively. We find that these numbers to be  $48.2 \pm 9.3\%$ ,  $5.4 \pm 3.1\%$ , and  $3.6 \pm 2.5\%$ . In comparison, we find significantly fewer stellar companions than Adams et al. (2012) at angular separations between  $0''.5$  to  $2''.0$ .

We therefore conduct a cross check with their targets, and find 20 overlapping targets. For these targets, we detect 40 companions using the images from the CFOP, while they detect 33 companions. We find 17 new companions that were not reported by Adams et al. (2012). Most of the new companions are more than  $6''$  away from central stars. We are not able to detect 10 of their companions. All of our missing detections have  $\Delta \text{Mag}$  larger than 7.1 mag (close to detection limit, see Fig. 2), and none of them are within  $2''$  except for KOI 18 ( $0''.9$  separation and  $\Delta \text{mag} = 5.0$ ). We suspect the difference may be a result of different thresholds for companion detections or differences in manual inspections.

We also conduct investigations on the lack of companion detections within  $2''.0$ . In the overlapping sample of 20 KOIs with Adams et al. (2012), we detect 2 companions within  $0''.5$ , KOI 292 ( $0''.43$ ), and KOI 975 ( $0''.72$ ). They are also detected in Adams et al. (2012), but KOI 18 with a separation of  $0''.9$  was missed in our search. For the overlapping sample,  $10.0 \pm 7.1\%$  (2 out of 20) have companions within  $2''$ . In comparison, for the rest of our sample, none of 36 stars has detected companions within  $2''$ , which raises a concern that KOIs with close-in companions may be filtered out when conducting RV followup observations. However, it does not seem to be the case for KOI 18, KOI 292, and KOI 975, these targets receive continued RV followup observations even after close-in companions are detected in AO images.

## 5. SUMMARY AND DISCUSSION

### 5.1. Summary

We conduct a search for stellar companions to a sample of 56 *Kepler* planet host stars, and compare the stellar multiplicity rate for planet host stars and the field stars in the solar neighborhood. We find that the stellar multiplicity rate for planet host stars is significantly lower than that for the field stars at stellar separations smaller than 1500 AU, indicating that planet formation is less efficient in multiple-star systems than in single stars. The influence of stellar companions plays a significant role in planet formation and evolution in multiple-star systems with separations smaller than 1500 AU.

We distinguish the planet occurrence rates for single and multiple-stars. We find that planets in S-type orbits in multiple-star systems are  $4.5 \pm 3.2$ ,  $2.6 \pm 1.0$ , and  $1.7 \pm 0.5$  times less frequent than planets orbiting single stars if a stellar companion is present at distances of 10, 100 and 1000 AU,

respectively. The difference in planet occurrence rate between single and multiple-star systems becomes insignificant when companions separation exceeds 1500 AU, suggesting that planet formation in widely-separated binaries is similar to that around single stars.

In summary, three improvements in this study allow us to better study planets in multiple-star systems. First, unlike planet host stars selected from ground-based RV and transiting surveys, our sample from the *Kepler* mission does not have strong bias against planets in multiple-star systems. Second, we combine the RV and AO data for the 56 *Kepler* stars, which construct a survey for stellar companions with high completeness. The DA method is also used to put further constraints on stellar companions in systems with multiple transiting planets. Third, we develop a method to quantify the detection bias of planets in multiple-star systems, which enables a fair comparison of stellar multiplicity rate.

### 5.2. Discussion

#### 5.2.1. Stellar Companions to Hot Jupiter Host Stars

There are 6 hot Jupiter (HJ,  $P < 10$  day and  $R_p > 5 R_{\oplus}$ ) host stars in our sample. They are KOI 5, KOI 10, KOI 17, KOI 18, KOI 20, and KOI 22. Four (67%) of them have detected stellar companions. The stellar multiplicity rate for HJ host stars is much higher than the rest of the sample, i.e., 32%. While we recognize the small number statistics and the possible non-association of these visual companions, this may imply that stellar companions play a role in HJ migration. Knutson et al. (2014) conducted a search for massive companions to close-in gas giant planets. They estimated an occurrence rate of  $51\% \pm 10\%$  for companions with masses between  $1-13 M_J$  and semi-major axes between 1-20 AU. The high occurrence rate for both massive sub-stellar companions and stellar companions may suggest that planet-planet and star-planet interactions have a comparable influence on the migration of HJs. Given the large separations of stellar companions ( $a > 1500$  AU), the Kozai timescales for all HJ systems with stellar companions (except for KOI 5) are  $\sim 10^8-10^9$  years, which are comparable to the age of the systems, and perhaps too long to effectively perturb the orbit of a gas giant planet. Therefore, it is still inconclusive whether the HJs in these systems migrate to their current positions due to the perturbation of the detected stellar companions.

#### 5.2.2. Stellar Multiplicity Rate For Single and Multiple Planet Systems

Perturbation from a companion star will change the mutual inclinations of planets in the same system (Wang et al. 2014, see also §3.3). We therefore expect to see a lower stellar multiplicity rate for stars with multiple transiting planets than stars with only one transiting planet. There are 27 stars in our sample with multiple transiting planets and 29 stars with only one transiting planet. Fig. 7 shows the comparison of stellar multiplicity rate for these two sub samples. The hatched regions

with different colors overlap, so there is no statistically significant difference in the stellar multiplicity rate between systems with multiple transiting planets and system with only one transiting planet. However, for separations between 50 and 1000 AU, we notice a relatively lower stellar multiplicity rate for multiple transiting planet systems than systems with only one detected transiting planet, suggesting that companion perturbations affect planet mutual inclination and/or multiple planet formation. An ongoing AO campaign is being carried out at the Palomar observatory to study the stellar multiplicity rate for multi-planet host stars, and will address the role of stellar perturbation in planet formation and detection.

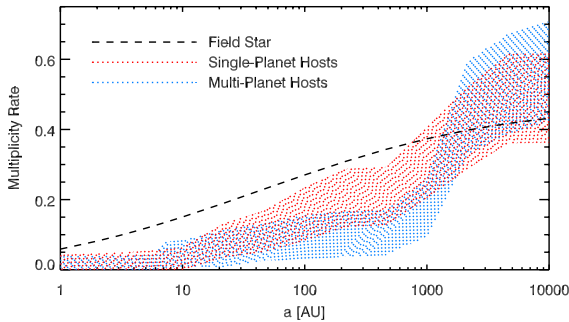


**Figure 7.** Comparison of stellar multiplicity rate for field stars (dashed line), 29 planet host stars with a single detected planet (red dotted region,  $1-\sigma$  range), 27 planet host stars with multiple detected planets (blue dotted region,  $1-\sigma$  range).

### 5.2.3. Needing a Better Control Sample Than the Field Stars

There are several uncertainties to use the field stars as a control sample to compare to the *Kepler* sample. First, it is uncertain that *Kepler* overall sample (i.e., all *Kepler* stars) multiplicity rate is the same as the field stars. *Kepler* stars are mainly selected by applying a magnitude cut (magnitude-limited), whereas the field stars are volume-limited (Duquennoy & Mayor 1991; Raghavan et al. 2010). Therefore, Malmquist bias exists for the *Kepler* stars, brighter, more distant stars, are selected, which include young stars, giant stars, and binary stars. While some young stars and giant stars can be excluded by applying a  $T_{\text{eff}}$  and  $\log(g)$  cut from the *Kepler* Input Catalog (KIC, Brown et al. 2011), it is more difficult to discern binary stars, so it is possible that the stellar multiplicity rate for *Kepler* stars could be higher than that of the field stars (Gaidos & Mann 2013).

The second uncertainty lies in the fraction of field stars with planets. We compare the stellar multiplicity rate for the field stars and planet host stars. Most of them are small planet host stars. However, the fraction of field stars hosting small planets is less constrained than the fraction of field stars hosting large planets (Howard et al. 2010). If (1) not all field stars have a planet; and (2) the statistics of multiple-stars (multiplicity, separation distribu-

tion, etc.) are comparable for the nearby solar-type stars and for the stars in our sample, then the difference in Fig. 5 should suggest the impact of stellar companions on planet occurrence. In this case, the field stars are a sample contaminated by planet host stars. If we see a difference when comparing a sample of planet host stars to the field stars, then the difference would have been more distinct when comparing the planet host sample and a non-planet host sample. The latter is difficult to obtain because of the limitation of current detection sensitivity. However, a planet mass or radius limit can be set to study a certain type of planet, e.g., comparing the stellar multiplicity rate for the giant planet host stars and stars without a gas giant planet. In this case, any difference in the multiplicity rate reflects the impact of stellar companions on gas giant planet formation.

**Acknowledgements** The authors thank Howard Isaacson and Matt Giguere for helpful comments and proofreading the paper. The research is made possible by the data from the Kepler Community Follow-up Observing Program (CFOP). The authors acknowledge all the CFOP users who uploaded the AO and RV data used in the paper. This research has made use of the NASA Exoplanet Archive, which is operated by the California Institute of Technology, under contract with the National Aeronautics and Space Administration under the Exoplanet Exploration Program. Jiwei Xie is supported by a Foundation for the Author of National Excellent Doctoral Dissertation (FANEDD) of PR China.

## REFERENCES

- Adams, E. R., Ciardi, D. R., Dupree, A. K., Gautier, III, T. N., Kulesa, C., & McCarthy, D. 2012, *AJ*, 144, 42
- Adams, E. R., Dupree, A. K., Kulesa, C., & McCarthy, D. 2013, *AJ*, 146, 9
- Batalha, N. M., et al. 2013, *ApJS*, 204, 24
- Bergfors, C., et al. 2013, *MNRAS*, 428, 182
- Bonavita, M., & Desidera, S. 2007, *A&A*, 468, 721
- Bonfils, X., et al. 2013, *A&A*, 549, A109
- Borucki, W. J., et al. 2011, *ApJ*, 736, 19
- Brown, T. M., Latham, D. W., Everett, M. E., & Esquerdo, G. A. 2011, *AJ*, 142, 112
- Burke, C. J., et al. 2014, *ApJS*, 210, 19
- Cochran, W. D., Hatzes, A. P., Butler, R. P., & Marcy, G. W. 1997, *ApJ*, 483, 457
- Cumming, A., Butler, R. P., Marcy, G. W., Vogt, S. S., Wright, J. T., & Fischer, D. A. 2008, *PASP*, 120, 531
- Daemgen, S., Hormuth, F., Brandner, W., Bergfors, C., Janson, M., Hippler, S., & Henning, T. 2009, *A&A*, 498, 567
- Demarque, P., Woo, J.-H., Kim, Y.-C., & Yi, S. K. 2004, *ApJS*, 155, 667
- Desidera, S., & Barbieri, M. 2007, *A&A*, 462, 345
- Doyle, L. R., et al. 2011, *Science*, 333, 1602
- Dressing, C. D., Adams, E. R., Dupree, A. K., Kulesa, C., & McCarthy, D. 2014, *ArXiv e-prints*
- Dressing, C. D., & Charbonneau, D. 2013, *ApJ*, 767, 95
- Duchêne, G., & Kraus, A. 2013, *ARA&A*, 51, 269
- Duquennoy, A., & Mayor, M. 1991, *A&A*, 248, 485
- Dvorak, R. 1982, *Oesterreichische Akademie Wissenschaften Mathematisch naturwissenschaftliche Klasse Sitzungsberichte Abteilung*, 191, 423
- Eggenberger, A., & Udry, S. 2007, *ArXiv e-prints*

- Eggenberger, A., Udry, S., Chauvin, G., Forveille, T., Beuzit, J.-L., Lagrange, A.-M., & Mayor, M. 2011, in IAU Symposium, Vol. 276, IAU Symposium, ed. A. Sozzetti, M. G. Lattanzi, & A. P. Boss, 409–410  
 Eggenberger, A., Udry, S., & Mayor, M. 2004, A&A, 417, 353  
 Feiden, G. A., & Chaboyer, B. 2012, ApJ, 757, 42  
 Fischer, D. A., & Marcy, G. W. 1992, ApJ, 396, 178  
 Fressin, F., et al. 2013, ApJ, 766, 81  
 Gaidos, E. 2013, ApJ, 770, 90  
 Gaidos, E., & Mann, A. W. 2013, ApJ, 762, 41  
 Giguere, M. J., et al. 2012, ApJ, 744, 4  
 Gilliland, R. L., Star, K. M., Adams, E. R., Ciardi, D. R., Kalas, P., & Wright, J. T. 2014, ArXiv e-prints  
 Ginski, C., Mugrauer, M., Seeliger, M., & Eisenbeiss, T. 2012, MNRAS, 421, 2498  
 Hale, A. 1994, AJ, 107, 306  
 Hayward, T. L., Brandl, B., Pirger, B., Blacken, C., Gull, G. E., Schoenwald, J., & Houck, J. R. 2001, PASP, 113, 105  
 Horch, E. P., Howell, S. B., Everett, M. E., & Ciardi, D. R. 2012, AJ, 144, 165  
 Horch, E. P., Veilleux, D. R., Baena Gallé, R., Shah, S. C., O’Rielly, G. V., & van Altena, W. F. 2009, AJ, 137, 5057  
 Howard, A. W., et al. 2010, Science, 330, 653  
 Huber, D., et al. 2014, ApJS, 211, 2  
 Jang-Condell, H. 2017, ApJ, 654, 641  
 Jenkins, J. M., et al. 2010a, ApJ, 713, L87  
 Jenkins, J. M., et al. 2010b, in Society of Photo-Optical Instrumentation Engineers (SPIE) Conference Series, Vol. 7740, Society of Photo-Optical Instrumentation Engineers (SPIE) Conference Series  
 Kane, S. R., et al. 2014, ApJ, 785, 93  
 Kley, W., & Nelson, R. P. 2008, A&A, 486, 617  
 Knutson, H. A., et al. 2013, ArXiv e-prints  
 —. 2014, ApJ, 785, 126  
 Konacki, M. 2005, ApJ, 626, 431  
 Konacki, M., Mutterspaugh, M. W., Kulkarni, S. R., & Helminiak, K. G. 2009, ApJ, 704, 513  
 Kopparapu, R. K. 2013, ApJ, 767, L8  
 Kraus, A. L., & Hillenbrand, L. A. 2007, AJ, 134, 2340  
 Kraus, A. L., Ireland, M. J., Hillenbrand, L. A., & Martinache, F. 2012, ApJ, 745, 19  
 Law, N. M., et al. 2013, ArXiv e-prints  
 Lillo-Box, J., Barrado, D., & Bouy, H. 2012, A&A, 546, A10  
 —. 2014, A&A, 566, A103  
 Lissauer, J. J., et al. 2011, ApJS, 197, 8  
 Lloyd, J. P., Liu, M. C., Macintosh, B. A., Sevenson, S. A., Deich, W. T., & Graham, J. R. 2000, in Society of Photo-Optical Instrumentation Engineers (SPIE) Conference Series, Vol. 4008, Optical and IR Telescope Instrumentation and Detectors, ed. M. Iye & A. F. Moorwood, 814–821  
 Luhman, K. L., & Jayawardhana, R. 2002, ApJ, 566, 1132  
 Mann, A. W., Gaidos, E., Lépine, S., & Hilton, E. J. 2012, ApJ, 753, 90  
 Marcy, G. W., et al. 2014, ApJS, 210, 20  
 Mayor, M., et al. 2011, ArXiv e-prints  
 Mugrauer, M., & Neuhäuser, R. 2009, A&A, 494, 373  
 Mugrauer, M., Neuhäuser, R., & Mazeh, T. 2007, A&A, 469, 755  
 Paardekoooper, S.-J., Thébault, P., & Mellema, G. 2008, MNRAS, 386, 973  
 Parker, R. J., & Quanz, S. P. 2013, MNRAS, 436, 650  
 Patience, J., et al. 2002, ApJ, 581, 654  
 Petigura, E. A., Howard, A. W., & Marcy, G. W. 2013, Proceedings of the National Academy of Sciences  
 Petigura, E. A., Marcy, G. W., & Howard, A. W. 2013, ApJ, 770, 69  
 Quintana, E. V., Adams, F. C., Lissauer, J. J., & Chambers, J. E. 2007, ApJ, 660, 807  
 Raghavan, D., Henry, T. J., Mason, B. D., Subasavage, J. P., Jao, W.-C., Beaulieu, T. D., & Hambly, N. C. 2006, ApJ, 646, 523  
 Raghavan, D., et al. 2010, ApJS, 190, 1  
 Roell, T., Neuhäuser, R., Seifahrt, A., & Mugrauer, M. 2012, A&A, 542, A92  
 Sarlot, R. J., McCarthy, D. W., Burge, J. H., & Ge, J. 1999, in Society of Photo-Optical Instrumentation Engineers (SPIE) Conference Series, Vol. 3779, Current Developments in Optical Design and Optical Engineering VIII, ed. R. E. Fischer & W. J. Smith, 274–283  
 Schwamb, M. E., et al. 2013, ApJ, 768, 127  
 Smith, J. A., et al. 2002, AJ, 123, 2121  
 Swift, J. J., Johnson, J. A., Morton, T. D., Crepp, J. R., Montet, B. T., Fabrycky, D. C., & Muirhead, P. S. 2013, ApJ, 764, 105  
 Thébault, P. 2011, Celestial Mechanics and Dynamical Astronomy, 111, 29  
 Thébault, P., Marzari, F., & Scholl, H. 2006, Icarus, 183, 193  
 Toyota, E., et al. 2009, PASJ, 61, 19  
 Vogt, S. S., et al. 1994, in Society of Photo-Optical Instrumentation Engineers (SPIE) Conference Series, Vol. 2198, Society of Photo-Optical Instrumentation Engineers (SPIE) Conference Series, 362–+  
 Wang, J., Xie, J.-W., Barclay, T., & Fischer, D. A. 2014, ApJ, 783, 4  
 Welsh, W. F., et al. 2012, Nature, 481, 475  
 Wizinowich, P. L., Acton, D. S., Lai, O., Gathright, J., Lupton, W., & Stomski, P. J. 2000, in Society of Photo-Optical Instrumentation Engineers (SPIE) Conference Series, Vol. 4007, Society of Photo-Optical Instrumentation Engineers (SPIE) Conference Series, ed. P. L. Wizinowich, 2–13  
 Wright, J. T., Marcy, G. W., Howard, A. W., Johnson, J. A., Morton, T. D., & Fischer, D. A. 2012, ApJ, 753, 160  
 Xie, J.-W., Zhou, J.-L., & Ge, J. 2010, ApJ, 708, 1566

**Table 1**  
RV and AO data for 56 KOIs

KOI	KIC	$\alpha$ (deg)	KOI $\delta$ (deg)	$K_P$ (mag)	$T_{\text{eff}}$ (K)	$\log g$ (cgs)	#PL	$T_{\text{start}}$ (MJD)	RV $T_{\text{end}}$ (MJD)	#RV	Telescope	AO
00005	8554498	289.739716	44.647419	11.665	5861.00	4.190	2	54983.516	56486.440	21	Keck Palomar	
00007	11853905	285.615326	50.135750	12.211	5858.00	4.280	1	55041.491	56134.480	22	Keck Palomar	
00010	6922244	281.288116	42.451080	13.563	6025.00	4.110	1	54983.540	55781.534	50	Palomar	
00017	10874614	296.837250	48.239944	13.303	5826.00	4.420	1	54984.561	55043.520	10	Palomar	
00018	8191672	299.407013	44.035053	13.369	6297.00	3.990	1	54985.594	55110.314	9	Gemini Gemini Palomar	
00020	11804465	286.243439	50.040379	13.438	6011.00	4.230	1	55014.412	55761.325	16	Palomar	
00022	9631995	282.629669	46.323360	13.435	5972.00	4.410	1	55014.403	55792.438	16	Palomar	
00041	6521045	291.385986	41.990269	11.197	5909.00	4.300	3	54988.511	56533.359	64	Keck Palomar	
00069	3544595	291.418304	38.672359	9.931	5593.00	4.510	1	55042.587	56547.339	61	Keck MMT MMT Palomar	
00070	6850504	287.697998	42.338718	12.498	5443.00	4.450	5	55073.386	56533.484	38	Palomar	
00072	11904151	285.679382	50.241299	10.961	5627.00	4.390	2	55073.400	56172.301	54	MMT MMT Palomar	
00082	10187017	281.482727	47.208031	11.492	4908.00	4.610	5	55311.579	56533.335	65	Keck MMT MMT	
00084	2571238	290.420807	37.851799	11.898	5541.00	4.530	1	55073.419	55723.450	20	Palomar	
00085	5866724	288.688690	41.151180	11.018	6172.00	4.360	3	55696.490	55738.516	6	MMT MMT	



Table 1 — Continued

KOI	KIC	$\alpha$ (deg)	KOI $\delta$ (deg)	$K_P$ (mag)	$T_{\text{eff}}$ (K)	$\log g$ (cgs)	#PL	$T_{\text{start}}$ (MJD)	RV $T_{\text{end}}$ (MJD)	#RV	Telescope	AO
00087	10593626	289.217499	47.884460	11.664	5510.00	4.500	1	55425.386	56521.486	26	Palomar Palomar	
00103	2444412	291.683350	37.751591	12.593	5531.00	4.440	1	55073.441	55797.539	16	Palomar	
00104	10318874	281.194733	47.497131	12.895	4786.00	4.590	1	55377.342	56525.316	30	Keck Palomar Palomar	
00108	4914423	288.984558	40.064529	12.287	5975.00	4.330	2	55073.469	56145.498	22	Keck Palomar	
00111	6678383	287.604614	42.166779	12.596	5711.00	4.410	4	55372.555	56521.442	14	Palomar	
00116	8395660	300.863983	44.337551	12.882	5865.00	4.410	4	55133.397	56532.332	33	Keck MMT	
00122	8349582	284.482452	44.398041	12.346	5714.00	4.390	1	55073.495	56151.511	33	Keck Palomar	
00123	5094751	290.392731	40.284870	12.365	5871.00	4.150	2	55074.492	56166.345	15	Keck Palomar	
00137	8644288	298.079437	44.746319	13.549	5385.00	4.430	3	55075.509	56146.484	20	Palomar	
00148	5735762	299.139221	40.949020	13.040	5190.00	4.490	3	55073.527	56532.436	43	Keck Palomar	
00153	12252424	287.997894	50.944328	13.461	4725.00	4.640	2	55313.592	56524.353	29	Keck MMT Palomar Palomar	
00157	6541920	297.115112	41.909142	13.709	5685.00	4.380	6	55440.501	56533.434	7	Palomar Robo-AO	
00180	9573539	284.394287	46.249081	13.024	5680.00	4.500	1	55074.466	55083.341	6	Palomar	
00244	4349452	286.638397	39.487881	10.734	6103.00	4.070	2	55366.603	56519.408	104	Keck Palomar Palomar	
00245	8478994	284.059540	44.518215	9.705	5288.00	4.590	4	55312.586	56523.237	59	Gemini Gemini Keck MMT MMT	
00246	11295426	291.032318	49.040272	9.997	5793.00	4.281	2	55312.582	56519.420	65	Keck MMT MMT	
00261	5383248	297.069611	40.525131	10.297	5692.00	4.420	1	55404.530	56518.546	36	Keck MMT MMT	
00263	10514430	281.273804	47.774399	10.821	5820.00	4.150	1	55395.529	55788.482	6	MMT MMT Palomar Palomar	
00265	12024120	297.018829	50.408981	11.994	6040.00	4.360	1	55782.522	56532.354	27	Gemini Gemini Palomar Palomar	
00273	3102384	287.478516	38.228840	11.457	5783.00	4.430	1	55431.309	56613.223	20	MMT MMT	
00274	8077137	282.492218	43.980209	11.390	6090.00	4.130	2	55403.447	56474.522	8	Gemini Gemini MMT MMT	
00283	5695396	288.530823	40.942299	11.525	5687.00	4.420	2	55433.368	56524.331	30	Keck Palomar Palomar	
00289	10386922	282.945648	47.574905	12.747	5812.00	4.458	2	56449.401	56532.291	5	Lick	
00292	11075737	287.326630	48.673431	12.872	5780.00	4.430	1	55377.475	56166.411	21	Keck Palomar Palomar	
00299	2692377	285.661652	37.964500	12.899	5538.00	4.340	1	55403.512	56530.414	32	Keck	
00305	6063220	297.354004	41.300049	12.970	4782.00	4.610	1	55403.543	56531.340	36	Keck	
00321	8753657	291.848053	44.968220	12.520	5538.00	4.340	2	55378.534	56493.368	47	Keck Lick	
00364	7296438	295.872314	42.881149	10.087	5798.00	4.240	1	55376.346	55699.442	3	WIYN	
00365	11623629	297.486908	49.623451	11.195	5451.00	4.490	2	55402.354	56532.377	24	Palomar Palomar	
00377	3323887	285.573975	38.400902	13.803	5777.00	4.450	3	55342.448	56506.363	16	Palomar Palomar	
00701	9002278	283.212738	45.349861	13.725	4807.00	4.690	5	56137.475	56507.530	15	Keck	
00975	3632418	287.361816	38.714016	8.224	6131.00	3.950	1	55439.438	56486.562	44	MMT MMT	
01431	11075279	287.022278	48.681938	13.460	5649.00	4.460	1	56472.391	56532.502	6	WIYN	
01439	11027624	290.851776	48.521339	12.849	5930.00	4.090	1	55075.273	56531.312	6	Lick	
01442	11600889	286.036346	49.614510	12.521	5476.00	4.448	1	55696.518	56446.424	17	Keck Lick	
01463	7672940	288.258636	43.376465	12.328	6020.00	4.380	1	56027.511	56530.292	3	WIYN	
01612	10963065	284.786194	48.423229	8.769	6027.00	4.220	1	55697.588	56494.420	42	Keck Lick	
01781	11551692	287.605591	49.523258	12.231	4977.00	4.590	3	56076.566	56112.331	9	Palomar Robo-AO	
01925	9955598	293.679199	46.852760	9.439	5365.00	4.430	1	55999.646	56547.332	40	Keck Palomar	
02169	9006186	285.207489	45.384350	12.404	5447.00	4.420	4	56099.455	56171.456	4	Palomar Robo-AO	
02687	7202957	292.615112	42.764252	10.158	5803.00	3.910	2	55999.652	56531.383	22	Palomar	
02720	8176564	295.439667	44.039162	10.338	6109.00	4.410	1	56018.575	56519.389	18	Keck Palomar	

Table 2  
RV measurement results for 56 KOIs.

KOI	KIC	$\text{RMS}_1^{**}$ (m·s <sup>-1</sup> )	$\delta v$ (m·s <sup>-1</sup> )	$\frac{\text{RMS}_1}{\delta v} > 5$	Slope	Non-transiting	$\text{RMS}_2^{***}$ (m·s <sup>-1</sup> )	$\frac{\text{RMS}_2}{\delta v} > 5$
00005*	8554498	94.9	4.2	✓		✓	23.7	✓
00007	11853905	7.9	2.1				4.5	
00010	6922244	53.8	13.2				47.1	
00017	10874614	57.8	3.6	✓			7.1	
00018	8191672	178.1	6.1	✓			18.2	
00020	11804465	44.5	4.1	✓			22.0	✓
00022	9631995	44.2	3.8	✓			40.9	✓
00041	6521045	5.4	1.6				5.4	
00069*	3544595	21.2	1.3	✓	✓		3.0	
00070	6850504	11.0	1.9	✓			10.2	✓
00072	11904151	4.6	1.6				3.7	
00082	10187017	4.5	1.2				4.2	
00084	2571238	11.2	1.8	✓			11.2	✓
00085	5866724	10.1	1.9	✓			15.5	✓
00087	10593626	5.0	1.6				4.8	
00103	2444412	6.8	1.9				6.2	
00104	10318874	96.1	2.0	✓		✓	6.1	
00108	4914423	7.6	2.2				7.4	
00111	6678383	6.1	2.6				6.6	

Table 2 — Continued

KOI	KIC	RMS <sub>1</sub> ** (m·s <sup>-1</sup> )	$\delta v$ (m·s <sup>-1</sup> )	$\frac{\text{RMS}_1}{\delta v} > 5$	Slope	Non-transiting	RMS <sub>2</sub> *** (m·s <sup>-1</sup> )	$\frac{\text{RMS}_2}{\delta v} > 5$
00116	8395660	6.5	2.4				6.5	
00122	8349582	5.1	1.7				4.7	
00123	5094751	7.1	2.4				6.9	
00137	8644288	9.7	2.5				8.0	
00148	5735762	32.7	2.3	✓		✓	14.2	✓
00153	12252424	9.7	2.4				8.9	
00157	6541920	36.7	8.1				49.9	✓
00180	9573539	15.7	2.1	✓			15.6	✓
00244	4349452	8.3	3.5			✓	6.5	
00245	8478994	5.0	1.3				3.3	
00246	11295426	16.9	1.3	✓		✓	3.6	
00261	5383248	5.2	1.5				5.3	
00263	10514430	11.1	3.2				13.9	
00265	12024120	4.7	1.8				4.5	
00273	3102384	91.7	1.4	✓			10.3	✓
00274	8077137	4.0	1.9				3.7	
00283	5695396	5.7	1.6				5.7	
00289	10386922	12.1	2.1	✓			12.1	✓
00292	11075737	6.2	2.3				4.5	
00299	2692377	6.6	1.9				6.0	
00305	6063220	5.8	1.7				5.6	
00321	8753657	4.3	1.7				4.0	
00364	7296438	51.3	0.3	✓			51.3	✓
00365	11623629	4.3	1.3				4.0	
00377	3323887	13.3	6.0				12.3	
00701	9002278	4.7	3.0				4.9	
00975	3632418	8.9	3.0				8.9	
01431	11075279	8.3	2.1				7.1	
01439	11027624	10.2	2.3				15.4	✓
01442	11600889	89.0	2.0	✓		✓	3.1	
01463	7672940	116.1	2.8	✓			116.1	✓
01612	10963065	4.1	1.5				4.0	
01781	11551692	21.7	1.4	✓			24.3	✓
01925	9955598	3.4	1.1				2.5	
02169	9006186	6.6	0.9	✓			6.6	✓
02687	7202957	9.2	1.3	✓			10.2	✓
02720	8176564	3.8	1.4				3.6	

**Note.** — \*: KOIs considered in multiple-star systems.  
See §3.2.4 and §3.2.5 for detailed discussions. \*\*: RMS of the RV measurements. \*\*\*: RMS after removing the linear trend or the long-period signal, and the RV signal caused by detected planet candidates.

**Table 3**  
Visual companion detections with AO data.

KOI	$\Delta$ Mag (mag)	Separation (arcsec)	Distance (AU)	Distance (pc)	Significance ( $\sigma$ )	PA (deg)
K00005	2.3 (Br- $\gamma$ )	0.14	40.9	$290.9^{+63.2}_{-19.4}$	28.2	308.9
K00010	6.8 ( <i>J</i> )	3.88	3663.9	$944.5^{+100.1}_{-139.1}$	22.0	89.3
K00017	3.9 ( <i>J</i> )	4.11	2130.7	$517.9^{+27.6}_{-28.4}$	206.2	39.5
K00018	3.9 ( <i>J</i> )	7.26	8241.0	$1135.9^{+84.4}_{-154.0}$	323.2	148.2
K00018	6.3 ( <i>J</i> )	9.68	10995.5	$1135.9^{+84.4}_{-154.0}$	32.1	344.7
K00018	6.6 ( <i>J</i> )	3.50	3971.8	$1135.9^{+84.4}_{-154.0}$	28.5	110.1
K00018	7.3 ( <i>J</i> )	5.09	5783.0	$1135.9^{+84.4}_{-154.0}$	14.1	211.3
K00018	7.7 ( <i>J</i> )	5.89	6693.3	$1135.9^{+84.4}_{-154.0}$	9.8	106.3
K00018	7.7 ( <i>J</i> )	10.82	12293.3	$1135.9^{+84.4}_{-154.0}$	7.7	222.1
K00018	7.3 ( <i>J</i> )	7.26	8241.0	$1135.9^{+84.4}_{-154.0}$	7.3	77.6
K00018	8.0 ( <i>J</i> )	9.69	11004.0	$1135.9^{+84.4}_{-154.0}$	6.6	339.2
K00018	8.2 ( <i>J</i> )	7.09	8059.2	$1135.9^{+84.4}_{-154.0}$	6.5	219.2
K00070	4.3 ( <i>J</i> )	3.79	1058.9	$279.5^{+15.3}_{-23.6}$	217.7	51.8
K00087	6.2 ( <i>J</i> ), 6.1 ( <i>K</i> )	5.49	956.9	$174.4^{+15.2}_{-12.1}$	78.2	177.2
K00087	7.4 ( <i>J</i> ), 6.6 ( <i>K</i> )	5.53	964.1	$174.4^{+15.2}_{-12.1}$	28.4	75.2
K00103	7.3 ( <i>J</i> )	9.81	2985.6	$304.4^{+29.0}_{-27.0}$	9.5	278.5
K00108	5.5 ( <i>J</i> )	9.52	3357.4	$352.7^{+36.0}_{-22.0}$	98.8	348.6

Table 3 — Continued

KOI	$\Delta$ Mag (mag)	Separation (arcsec)	(AU)	Distance (pc)	Significance ( $\sigma$ )	PA (deg)
K00108	7.2 ( <i>J</i> )	5.00	1764.4	$352.7^{+36.0}_{-22.0}$	21.5	112.5
K00108	7.2 ( <i>J</i> )	2.51	887.0	$352.7^{+36.0}_{-22.0}$	19.9	74.8
K00108	7.4 ( <i>J</i> )	3.23	1139.2	$352.7^{+36.0}_{-22.0}$	18.2	100.9
K00108	7.4 ( <i>J</i> )	8.90	3139.4	$352.7^{+36.0}_{-22.0}$	17.1	19.2
K00111	7.5 ( <i>J</i> )	7.13	2052.6	$297.8^{+26.0}_{-29.1}$	10.8	117.7
K00111	7.8 ( <i>J</i> )	9.07	2702.5	$297.8^{+26.0}_{-29.1}$	7.7	175.5
K00111	8.2 ( <i>J</i> )	6.70	1995.1	$297.8^{+26.0}_{-29.1}$	8.2	96.0
K00116	3.8 ( <i>K</i> )	8.00	2907.0	$363.2^{+56.7}_{-40.3}$	164.1	353.5
K00116	4.8 ( <i>K</i> )	12.96	4707.6	$363.2^{+56.7}_{-40.3}$	51.9	144.3
K00116	6.2 ( <i>K</i> )	7.46	2710.6	$363.2^{+56.7}_{-40.3}$	18.1	107.1
K00116	6.3 ( <i>K</i> )	13.51	4907.8	$363.2^{+56.7}_{-40.3}$	13.2	113.8
K00116	6.3 ( <i>K</i> )	13.05	4740.8	$363.2^{+56.7}_{-40.3}$	12.7	357.4
K00116	7.5 ( <i>K</i> )	10.93	3969.3	$363.2^{+56.7}_{-40.3}$	7.5	19.7
K00116	7.3 ( <i>K</i> )	5.79	2101.4	$363.2^{+56.7}_{-40.3}$	6.3	141.1
K00122	6.7 ( <i>J</i> )	4.23	1446.2	$341.7^{+28.1}_{-30.3}$	30.0	211.3
K00123	5.2 ( <i>J</i> )	9.52	4749.5	$498.7^{+25.0}_{-99.9}$	62.3	198.8
K00123	6.4 ( <i>J</i> )	10.19	5083.7	$498.7^{+25.0}_{-99.9}$	19.2	95.2
K00137	5.9 ( <i>J</i> )	5.64	2471.4	$438.2^{+37.6}_{-41.0}$	44.4	350.7
K00137	7.8 ( <i>J</i> )	7.13	3122.2	$438.2^{+37.6}_{-41.0}$	7.6	185.5
K00137	7.9 ( <i>J</i> )	5.11	2240.3	$438.2^{+37.6}_{-41.0}$	6.6	136.2
K00148	3.5 ( <i>J</i> )	4.44	1369.1	$308.7^{+27.0}_{-17.2}$	519.8	220.6
K00148	5.4 ( <i>J</i> )	10.99	3391.9	$308.7^{+27.0}_{-17.2}$	77.0	230.1
K00148	5.5 ( <i>J</i> )	2.54	785.2	$308.7^{+27.0}_{-17.2}$	69.7	245.8
K00148	6.3 ( <i>J</i> )	8.05	2486.4	$308.7^{+27.0}_{-17.2}$	35.5	244
K00148	7.4 ( <i>J</i> )	6.06	1870.7	$308.7^{+27.0}_{-17.2}$	13.9	238.8
K00153	6.0 ( <i>K</i> )	8.01	1812.0	$226.2^{+18.6}_{-15.1}$	11.2	353.4
K00153	6.9 ( <i>J</i> ), 7.6 ( <i>K</i> )	6.17	1395.3	$226.2^{+18.6}_{-15.1}$	4.5	298.4
K00244	2.7 ( <i>J</i> ), 2.0 ( <i>K</i> )	8.40	2741.0	$326.3^{+23.4}_{-23.4}$	3231.4	287.6
K00244	7.6 ( <i>J</i> ), 7.0 ( <i>K</i> )	8.38	2733.6	$326.3^{+23.4}_{-44.6}$	27.5	101.4
K00263	1.0 ( <i>J</i> ), 1.0 ( <i>K</i> )	3.28	788.5	$240.7^{+17.7}_{-38.9}$	2430.8	268.2
K00273	6.2 ( <i>J</i> ), 5.6 ( <i>K</i> )	5.02	1201.8	$239.6^{+14.7}_{-15.2}$	32.6	344.0
K00283	7.9 ( <i>K</i> )	6.09	1266.2	$208.0^{+21.4}_{-11.2}$	7.0	271.4
K00289	8.6 ( <i>J</i> )	5.86	2201.2	$375.9^{+355.0}_{-69.8}$	5.1	88.3
K00289	7.7 ( <i>J</i> )	3.18	1195.0	$375.9^{+355.0}_{-69.8}$	6.1	308.6
K00292	4.2 ( <i>K</i> )	0.43	154.9	$358.5^{+40.9}_{-28.3}$	43.2	119.4
K00365	7.7 ( <i>J</i> ), 6.6 ( <i>K</i> )	7.12	1129.9	$158.8^{+15.1}_{-19.7}$	13.3	313.7
K00377	5.0 ( <i>J</i> ), 4.8 ( <i>K</i> )	6.02	3721.9	$617.9^{+48.5}_{-46.7}$	133.8	91.9
K00377	6.0 ( <i>J</i> ), 6.9 ( <i>K</i> )	8.04	4969.8	$617.9^{+48.5}_{-46.7}$	18.1	221.9
K00377	6.2 ( <i>J</i> ), 7.3 ( <i>K</i> )	2.88	1780.8	$617.9^{+48.5}_{-46.7}$	12.3	37.5
K00975	3.8 ( <i>J</i> ), 4.0 ( <i>K</i> )	0.73	90.4	$123.7^{+7.7}_{-17.9}$	31.2	133.4
K01442	4.7 ( <i>J</i> )	2.11	637.4	$302.3^{+18.0}_{-20.3}$	25.3	76.3
K01442	8.0 ( <i>J</i> )	5.69	1718.6	$302.3^{+18.0}_{-20.3}$	5.8	90.2

Table 4  
Detection Bias of Planets in Multiple Stars.

KOI	Period (day)	$R_P$ ( $R_\oplus$ )	$R_*$ ( $R_\odot$ )	$M_*$ ( $M_\odot$ )	Duration (hr)	CDPP* (ppm) <sub>eff</sub>	Quarters	$\alpha^{**}$
K00005	4.78033	5.66	1.42	1.15	2.01	36.3	17	0.930
K00007	3.21366	3.72	1.27	1.12	4.11	53.1	14	0.850
K00010	3.52250	15.90	1.56	1.14	3.20	136.0	17	0.961
K00017	3.23470	11.07	1.08	1.14	3.60	103.5	14	0.946
K00018	3.54847	17.40	2.02	1.45	4.08	102.7	17	0.619
K00020	4.43796	17.60	1.38	1.17	4.67	106.1	14	0.961
K00022	7.89145	11.27	1.11	1.16	3.79	82.4	17	0.938



Table 4 — Continued

KOI	Period (day)	$R_P$ ( $R_\oplus$ )	$R_*$ ( $R_\odot$ )	$M_*$ ( $M_\odot$ )	Duration (hr)	CDPP* <sub>eff</sub> (ppm)	Quarters	$\alpha^{**}$
K00041	12.81570	2.08	1.23	1.11	6.54	26.6	17	0.635
K00069	4.72675	1.50	0.87	0.89	2.93	17.9	17	0.938
K00070	10.85410	3.17	0.94	0.90	3.82	57.1	17	0.930
K00072	0.83749	1.37	1.00	0.91	1.80	29.6	14	0.938
K00082	16.14570	2.54	0.74	0.80	3.75	39.4	17	0.946
K00084	9.28701	2.53	0.86	0.91	3.54	34.3	17	0.938
K00085	5.85993	2.36	1.20	1.21	4.11	29.0	17	0.624
K00087	289.86200	2.10	0.85	0.83	7.40	23.4	17	0.773
K00103	14.91080	2.95	0.95	0.91	3.31	73.7	17	0.906
K00104	2.50806	3.36	0.76	0.81	1.14	84.9	17	0.961
K00108	15.96530	2.94	1.21	1.16	4.65	32.2	17	0.629
K00111	11.42750	2.14	0.93	0.81	4.59	47.5	17	0.930
K00116	13.57070	2.47	1.04	1.00	3.25	59.2	17	0.803
K00122	11.52310	2.78	1.09	1.07	4.06	45.2	17	0.773
K00123	6.48167	2.64	1.43	1.06	3.63	40.9	17	0.874
K00137	14.85890	6.01	0.98	0.94	3.63	83.8	17	0.954
K00148	9.67393	3.15	0.89	0.88	4.40	72.8	17	0.930
K00153	8.92511	2.47	0.69	0.74	2.77	91.0	17	0.938
K00157	31.99550	4.18	1.06	0.98	4.27	77.1	17	0.906
K00180	10.04560	2.53	0.92	0.99	3.26	62.0	17	0.866
K00244	12.72040	6.51	1.66	1.19	2.83	28.4	17	0.898
K00245	39.79220	1.94	0.73	0.75	4.57	17.3	17	0.946
K00246	5.39877	2.53	1.24	1.07	3.56	22.0	17	0.922
K00261	16.23850	2.65	1.02	0.99	3.86	36.0	17	0.914
K00263	20.71940	2.02	1.41	1.01	4.23	49.2	17	0.658
K00265	3.56806	1.29	1.18	1.16	3.43	36.1	17	0.528
K00273	10.57380	1.82	1.07	1.12	1.74	30.4	17	0.624
K00274	15.09200	1.13	1.55	1.20	4.14	28.0	17	0.500
K00283	16.09190	2.41	1.03	1.02	2.93	31.4	17	0.874
K00289	296.63700	5.04	0.95	0.94	16.43	28.3	17	0.930
K00292	2.58663	1.64	0.98	0.94	2.37	53.9	14	0.874
K00299	1.54168	1.98	1.11	0.99	1.94	84.7	17	0.890
K00305	4.60356	1.57	0.73	0.79	2.40	74.9	17	0.898
K00321	2.42631	1.50	1.11	0.99	2.65	50.7	17	0.850
K00364	173.92800	0.93	1.35	1.15	2.64	23.0	17	0.500
K00365	81.73750	2.29	0.87	0.85	6.78	23.7	17	0.906
K00377	19.27390	8.28	1.01	1.05	4.16	129.3	17	0.930
K00701	18.16410	1.91	0.60	0.65	2.96	83.3	17	0.922
K00975	2.78582	1.72	2.04	1.36	3.41	24.1	17	0.500
K01431	345.16100	8.45	1.00	1.06	7.50	45.8	14	0.890
K01439	394.61100	7.80	1.65	1.23	24.61	15.3	17	0.635
K01442	0.66934	1.23	0.99	1.01	1.29	54.7	14	0.795
K01463	580.00000	16.29	1.09	1.05	11.43	38.6	17	0.961
K01612	2.46503	0.78	1.31	1.05	1.19	16.7	14	0.629
K01781	7.83445	3.76	0.76	0.82	3.00	80.5	14	0.946
K01925	68.95800	1.12	0.95	0.88	2.99	15.4	17	0.658
K02169	5.45300	0.97	0.93	0.82	2.24	43.2	17	0.723
K02687	1.71683	1.90	1.94	1.12	2.11	24.2	17	0.818
K02720	6.57148	0.80	1.05	1.05	3.07	22.6	17	0.619

**Note.** — \*: effective combined differential photometric precision (Jenkins et al. 2010b). \*\*: correction factor for the bias against planet detection in binary stars. The factor ranges from 0 to 1, with 1 indicating 100% detection rate even with the flux contamination from a companion star. See §4.1 for more details.

**Table 5**  
Ratio of planet occurrence rate between single stars and multiple-star systems as a function of stellar separation.

$a$ (AU)	$f_s/f_m$	$\delta f_s/f_m^*$
1.0	12.94	...
2.0	12.87	...
5.0	11.21	...
10.0	4.52	3.16
21.5	2.99	1.53
46.4	2.84	1.29
100.0	2.55	1.01
215.4	2.43	0.89
464.2	2.75	0.99
1000.0	1.84	0.57
2154.4	0.87	0.23
4641.6	0.69	0.18
10000.0	0.68	0.18

**Note.** — \*: Error bars are calculated based on Poisson statistics and propagated through Equation 5. No error bar is given within 10 AU because of less than 1 detection of stellar companion according to Equation 3.